JOURNAL OF NANO AND MATERIALS SCIENCE RESEARCH
Volume 2, No.1 (Maiden edition, 2023), pp. 104 – 109
Available online at journals.nanotechunn.com/jnmsr

ORIGINAL ARTICLE

Impact of Transition Metal Doped Bismuth Oxide Nanocomposites on the Bandgap Energy for Photoanode Application

Shahbaz Afzal[a,e], Sidra Tehreem[b], Tahir Munir[b,e], Sakhi G. Sarwar[c,e], Imosobomeh L. Ikhioya[d,e,]*

[a]*Department of Physics, University of Education Lahore, DG Khan Campus 32200, Pakistan*
[b]*Institute of Physics, Baghdad ul Jadeed Campus, The Islamia University of Bahawalpur, Bahawalpur 63100, Pakistan.*
[c]*Centre of Excellence in Solid-State Physics, University of the Punjab, Lahore, Pakistan*
[d]*Department of Physics and Astronomy, University of Nigeria Nsukka, 410001, Nigeria*
[e]*National Centre for Physics, Quaid-i-Azam University Campus, Islamabad, 44000, Pakistan*

KEYWORDS

Doping,
Bandgap,
Metal oxide,
Bi_2O_3,
Photoanode

ARTICLE HISTORY

Received: May 25, 2023
Revised: June 11, 2023
Accepted: June 13, 2023
Published: July 31, 2023

ABSTRACT

Chemical co-precipitation approach has been successfully used to synthesize Bi_2O_3 and Zn/Bi_2O_3 nanoparticles. Bi_2O_3 exhibited a band gap energy of 1.78 eV, and Zn/Bi_2O_3 at 1 & 5% and band gaps of 1.83 eV & 1.99 eV respectively. The statistics unambiguously demonstrate that adding zinc dopant widens the energy gap. The cubic lattice structure of this crystal is produced by a powerful synergy between the zinc ions and bismuth oxide ions. The peaks showed well-aligned conspicuous diffraction peaks of the material with crystalline peaks at the (110) plane. The Bi_2O_3 patterns verified that the cubic crystal structure was successfully formed. With a classified orientation at the (110) plane, the synthesized material showed prominent peaks. The most noticeable peaks, with a strong orientation on the (110) plane, were recorded by the bismuth oxide material that was 1% doped. The FTIR peak at 811 cm^{-1} indicates association with the Bi-O bond, thus verifying the existence of bismuth oxide. Additionally, the peak at 1394 cm^{-1} corresponds to the C-H bond. The stretching vibrations of O-H were detected within the range of 3200 to 3445 cm^{-1}. The presence of a peak at 1635 cm^{-1} indicates the utilization of H_2O in the experimental procedure, while vibrations of water molecules are observed in the range of 2311 to 2331 cm^{-1}.

1 Introduction

Due to its wide range of possible applications in numerous fields, including sensors, supercapacitors, photovoltaics, photoanode, and photocatalysis, bismuth oxide has attracted substantial attention in scientific research [1].

Several methods have been used to synthesize the bismuth oxide. These include electrodeposition [2], chemical vapor deposition [3], thermal decomposition [4], sol-gel [5], flame spray pyrolysis [6], laser ablation [7], microwave [8], hydrothermal [9], solvothermal [10], solution combustion [11], thermal oxidation [12], and co-precipitation method [13].

Co-precipitation among all these methods is highly preferred. Using this method, the size of the nanoparticles can be controlled efficiently. It is the most convenient, inexpensive, and industrially viable technique for the preparation of NPs [14]. Among other metal semiconductor materials [15]–[27], bismuth oxide material has a wide range of application with excellent optical and structural properties.

A p-type semiconductor with a direct band gap of 2.8 eV is bismuth oxide. Unfortunately, when utilized alone, Bi_2O_3 shows little activity under visible light [28]. To enhance the visible light activity of Bi_2O_3 and improve the material's optical characteristics, it is therefore of significant interest to dope this material.

* **CORRESPONDING AUTHOR** | I. L. Ikhioya, ✉ imosobomeh.ikhioya@unn.edu.ng

Furthermore, when evaluating these materials for optoelectronic applications, the bandgap of Bi_2O_3 is quite important. Bismuth oxide has been seen to change into a major transition metal oxide with a variety of desirable characteristics when dopants are added. Doped bismuth oxide has a lot of promise for use in optical coatings, sensors, electrolyzes, ceramic membranes, solar cells, fuel cells, transparent ceramic glass production, and ceramic membranes.

As a result, the precise tuning of the bandgap in bismuth oxide depends critically on the presence of dopants [29]. Lithium [30], cerium [31], coumarin [32], ytterbium [33], vanadium [34], dysprosium and tantalum [35], and rare earth metals [28] have all been used as dopants in attempts to dope Bi_2O_3 for a range of purposes.

The objective of the current work is to use the chemical co-precipitation approach to examine the impact of transition metal zinc doping on the structural and optical characteristics of bismuth oxide. To do this, both the pure and doped nanoparticles have been examined using a variety of characterization techniques, such as X-ray Diffraction (XRD), Fourier Transform Infrared Spectroscopy (FTIR), and UV-visible Spectroscopy. These methods enable a thorough investigation of the structural and optical modifications brought about by the zinc doping procedure in bismuth oxide.

2 Experimental Section

2.1 Materials

As starting materials, sodium hydroxide (NaOH), zinc acetate ($Zn(CH_3COO)_2.2H_2O$), and bismuth nitrate ($Bi_2(NO_3)_2.5H_2O$) were all employed. All the chemicals were of analytical grade and used as received from Sigma-Aldrich.

2.2 Synthesis of Zn-doped Bismuth Oxide Nanocomposites

Zinc-doped (1 and 5 mol %) Bi_2O_3 was made by mixing 30 mL of deionized water with 1 M bismuth nitrate. After that, 30 mL of deionized water containing the stoichiometric amount of zinc acetate was added while being stirred magnetically.

Additionally, the above-mentioned solution had 30 mL of deionized water and 0.1 M NaOH dissolved in it added dropwise while being stirred. A light-yellow precipitate formed after being magnetically agitated for 5 hours at 80 °C with this mixed solution. The precipitate was then filtered after being repeatedly rinsed with deionized water. To create Zn-doped (1 and 5 mol%) Bi_2O_3 NPs, the precipitate was first dried for two hours at 100 °C in an oven and then further annealed for three hours at 500 °C in a muffle furnace. The same procedure was used to make pure Bi_2O_3 NPs without the use of zinc acetate.

3 Results and Discussions

3.1 Optical study of Bi_2O_3 and Zn/Bi_2O_3

Figure 1 displays the plots of the absorbance, transmittance, and reflectance data for the produced nanoparticles at various zinc dopant molarities. All of the produced nanoparticles showed a similar pattern in the absorbance plot (Figure 1(S1)), with elevated absorbance data in the UV region and a drop in absorbance as the wavelength moved toward the visible-near infrared region.

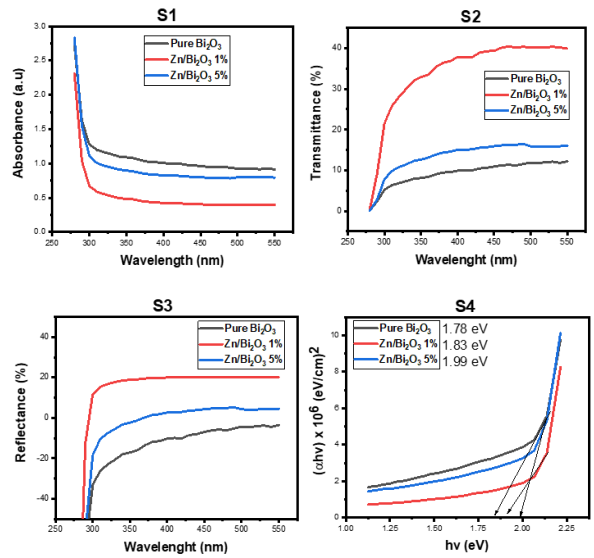

Figure 1: (S1-absorbance), (S2-transmittance), (S3-reflectance), and (S4-bandgap energy)

In comparison to undoped Bi_2O_3, it was discovered that adding a small amount of zinc (1%) as a dopant reduced the absorbance of the Bi_2O_3 nanoparticles throughout the electromagnetic spectrum. Even beyond the (1%) doped zinc absorbance data, further increases in the zinc dopant (to 5%) dramatically enhance the absorbance data. The absorbance of the material rises with increasing electromagnetic light radiation and zinc molar concentration, which causes an increase in the absorbance of Zn/Bi_2O_3 at high doping levels. Bi_2O_3 doped with 5% zinc has a strong UV absorbance, which makes the material appropriate for p-n junction formation in solar cells and photovoltaic applications in general. Equation (1) was used to extrapolate the absorbance result to the transmittance data for all nanoparticles.

$$T = 10^{-A} \quad (1)$$

Figure 1(S2) depicts the transmittance plot of pure Bi_2O_3 and Zn/Bi_2O_3 nanoparticles produced at various zinc dopant molarities. The 1% transmittance rose as the wavelength increased in all synthesized nanoparticles, showing a consistent pattern. Bi_2O_3 materials were found to have much lower transmittance data when a higher concentration of zinc dopant (5%) was added, notably in the visible-near-infrared region. This makes it a good material for solar energy collectors and optical devices.

Figure 1(S3) shows the graphical data of the reflectance versus wavelength for materials produced from Bi_2O_3 and Zn/Bi_2O_3 at different zinc dopant molarities. It appears that Zn/Bi_2O_3 and Bi_2O_3 have low reflecting properties. Most materials' low

reflectivity makes them suitable for anti-reflective coatings and a potential component of solar control coatings.

The energy band gap (E_g) of Bi_2O_3 and Zn/Bi_2O_3 at varied zinc dopant molarity was deduced via Equation (2).

$$(\alpha h\nu)^2 = A(h\nu - E_g) \quad (2)$$

Figure 1 (S4) shows a plot of $(\alpha h\nu)^2$ against $h\nu$ for Bi_2O_3 and Zn/Bi_2O_3 at varied zinc dopant molarity. The materials' energy band gap was calculated from this plot by projecting the straight section of the curve down to the hv axis at $(\alpha h\nu)^2 = 0$. Bi_2O_3 exhibited a band gap energy of 1.78 eV, and Zn/Bi_2O_3 at 1% & 5% had band gaps of 1.83 eV & 1.99 eV respectively. The statistics unambiguously demonstrate that adding zinc dopant widens the energy gap. Bi_2O_3 and Zn/Bi_2O_3 are excellent promising materials for solar cell manufacturing, according to band gap statistics.

3.2 *Structural study of Bi_2O_3 and Zn/Bi_2O_3*

The synthesized nanoparticles' structural layout is shown in Figure 2. The cubic crystal structure in Figure 2's X-ray diffractograms has the JCPDS card number 01-074-2276. The cubic lattice structure of this crystal is produced by a powerful synergy between the zinc ions and bismuth oxide ions.

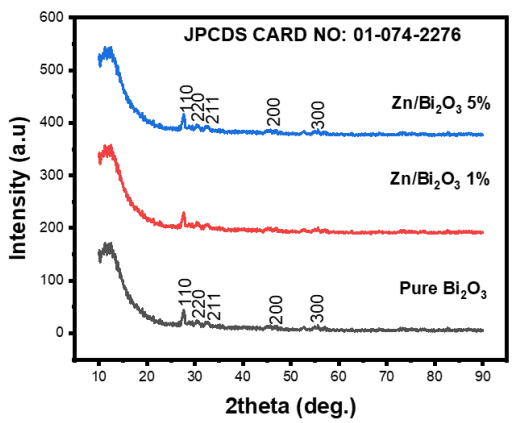

Figure 2: XRD patterns of Bi_2O_3 and Zn/Bi_2O_3

The peaks showed well-aligned conspicuous diffraction peaks of the material with crystalline peaks at the (110) plane. The Bi_2O_3 patterns verified that the cubic crystal structure was successfully formed. With a classified orientation at the (110) plane, the synthesized material showed prominent peaks.

The most noticeable peaks, with a strong orientation on the (110) plane, were recorded by the bismuth oxide material that was 1% doped. Due to the modest ionic size of the zinc, the addition of zinc does not significantly alter the crystal structure; therefore, there is no discernible peak shift.

The material's crystallite size, D, the lattice constants (a), the interplanar distance (d), and the dislocation densities, ($1/D^2$) as indicated in Table 1, were all calculated using Scherrer's equation ($D = k\lambda/\beta\cos\theta$). The variable lattice constants and dislocation densities were explained by the introduction of zinc and different crystallite sizes. The 2theta values rise and the lattice constant values change as a result of changes in the lattice sites brought on by an increase in crystallite size.

It has also been demonstrated that the lattice planes' interplanar distance varies over the orientation plane. The lattice structure changes as a result of distortions brought on by the introduction of the zinc, which allows the dopant to occupy the interstitial location. Peak broadening at larger 2theta values is explained by these aberrations.

3.3 *FTIR Analysis*

In the spectrum of Bi_2O_3, as depicted in Figure 3(S5), the occurrence of the peak at 811 cm^{-1} indicates the association with the Bi-O bond, thus verifying the existence of bismuth oxide.

Additionally, the peak at 1394 cm^{-1} corresponds to the C-H bond [36]. The stretching vibrations of O-H were detected within the range of 3200 to 3445 cm^{-1}. The presence of a peak at 1635 cm^{-1} indicates the utilization of H_2O in the experimental procedure, while vibrations of water molecules are observed in the range of 2311 to 2331 cm^{-1}.

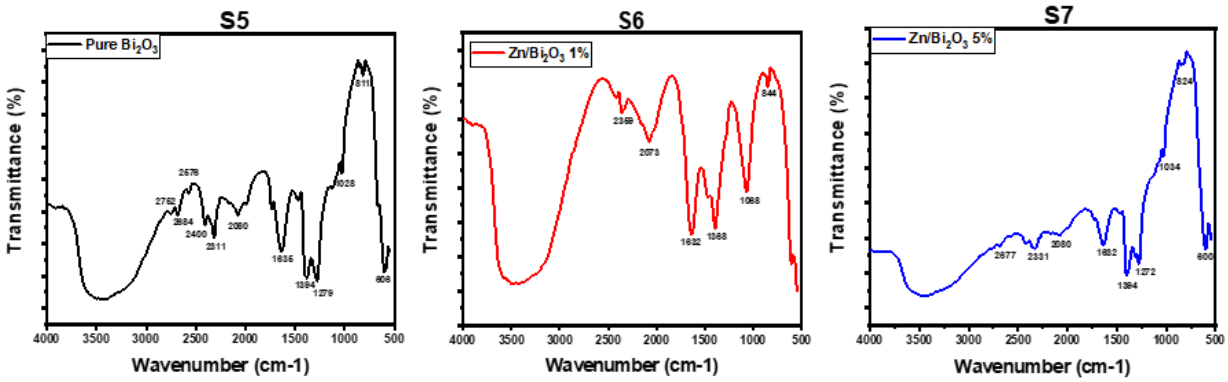

Figure 3: (S5-FTIR of Bi_2O_3), (S6- FTIR of Zn/Bi_2O_3 1%), and (S7- FTIR of Zn/Bi_2O_3 5%)

Table 1: Structural parameters of Bi_2O_3 and Zn/Bi_2O_3

Films	2θ (deg.)	Å	(Å)	(β)	(hkl)	D (nm)	σ (lines/m^2 × 10^{16})
Pure Bi_2O_3	27.36	3.256	5.640	2.0987	110	0.679	6.588
	30.38	2.939	5.878	2.0873	220	0.688	6.429
	32.66	2.739	5.478	2.0734	211	0.696	6.273
	47.04	1.930	4.315	2.0721	200	0.729	5.719
	55.60	1.651	4.045	2.0453	300	0.766	5.186
Zn/Bi_2O_3 1%	27.48	3.242	5.616	3.3313	110	0.428	1.659
	30.40	2.937	5.875	3.3311	220	0.431	1.637
	32.68	2.737	5.475	3.3310	211	0.433	1.618
	47.08	1.928	4.312	3.3291	200	0.454	1.475
	55.66	1.649	4.041	3.3288	300	0.471	1.373
Zn/Bi_2O_3 5%	27.48	3.242	5.616	3.4313	110	0.415	1.760
	30.40	2.937	5.875	3.4311	220	0.418	1.737
	32.68	2.737	5.475	3.4310	211	0.421	1.717
	47.08	1.928	4.312	3.4291	200	0.441	1.565
	55.66	1.649	4.041	3.4288	300	0.457	1.456

Table 2: Summary of observed FTIR peaks

S/No.	Wavenumber cm^{-1}	Information
1	3000-3444	O-H stretching
2	2311-2331	Vibration of water molecules
3	1635	Water
4	1394	C-H bond
5	811	Bi-O bond vibration

Furthermore, the peak observed at 1261 cm^{-1} can be attributed to the nitrate (NO^{3-}) group [37]. Apart from slight shifts in the wavenumbers, there is minimal distinction between undoped Bi_2O_3 and Zn/Bi_2O_3 (5%) nanoparticles. However, the Zn/Bi_2O_3 (1%) nanoparticles exhibit more pronounced O-H stretching within the range of 3000 – 3444 cm^{-1}, which is not observed in the undoped Bi_2O_3 or Zn/Bi_2O_3 (5%) samples. The observed FTIR peaks are presented in Table 2.

The FTIR spectrum shows that the peaks in Zn/Bi_2O_3 (1%) exhibit broadening, while there is a resemblance to undoped Bi_2O_3 as the zinc concentration in the nanoparticles increases to 5%. This behavior suggests a reduction in the crystallinity of the nanoparticles with an increasing concentration of zinc.

Additionally, the introduction of Zn doping leads to the emergence of an absorption peak in the visible region. This observation, as seen in Zn/Bi_2O_3 (1%), indicates that Zn doping has significantly improved the ability of Bi_2O_3 nanostructures to absorb visible light, thereby highlighting their potential for applications related to visible light-induced phenomena. These absorbance peaks due to doping can be attributed to transitions involving the dopant and the bismuth ions [29].

4 Conclusion

We have successfully used the chemical co-precipitation approach to synthesized Bi_2O_3 and Zn/Bi_2O_3. In comparison to undoped Bi_2O_3, it was discovered that adding a small amount of zinc (1%) as a dopant reduced the absorbance of the Bi_2O_3 nanoparticles throughout the electromagnetic spectrum. Even beyond the (1%) doped zinc absorbance data, further increases in the zinc dopant (to 5%) dramatically enhance the absorbance data. The 1% transmittance rose as the wavelength increased in all synthesized nanoparticles, showing a consistent pattern. Bi_2O_3 materials were found to have much lower transmittance data when a higher concentration of zinc dopant (5%) was added, notably in the visible-near-infrared region. Bi_2O_3 exhibited a band gap energy of 1.78 eV, and Zn/Bi_2O_3 at 1% & 5% had band gaps of 1.83 eV & 1.99 eV. The statistics unambiguously demonstrate that adding zinc dopant widens the energy gap. The cubic lattice structure of this crystal is produced by a powerful synergy between the zinc ions and bismuth oxide ions. The peaks showed well-aligned conspicuous diffraction peaks of the material with crystalline peaks at the (110) plane. The Bi_2O_3 patterns verified that the

cubic crystal structure was successfully formed. With a classified orientation at the (110) plane, the synthesized material showed prominent peaks. The most noticeable peaks, with a strong orientation on the (110) plane, were recorded by the bismuth oxide material that was 1% doped. the occurrence of the peak at 811 cm^{-1} indicates the association with the Bi-O bond, thus verifying the existence of bismuth oxide. Additionally, the peak at 1394 cm^{-1} corresponds to the C-H bond [23]. The stretching vibrations of O-H were detected within the range of 3200 to 3445 cm^{-1}. The presence of a peak at 1635 cm^{-1} indicates the utilization of H_2O in the experimental procedure, while vibrations of water molecules are observed in the range of 2311 to 2331 cm^{-1}.

Authors' Credit Statement

Shahbaz Afzal, Sidra Tehreem, Tahir Munir, Sakhi G. Sarwar: Original draft writing, methodology, reviewing and editing, conceptualization, data curation, software, **Shahbaz Afzal and Imosobomeh L. Ikhioya**: data collection, first-draft writing, conceptualization, data collection, methodology, software, reviewing, and editing, **Tahir Munir, Sakhi G. Sarwar, Imosobomeh L. Ikhioya**: visualization, data curation

Declaration of Competing Interest

Authors have declared no existing conflict of interest.

References

[1] M. J. Jabeen Fatima, A. Navaneeth, and S. Sindhu, “Improved carrier mobility and bandgap tuning of zinc doped bismuth oxide,” *RSC Adv*, vol. 5, no. 4, pp. 2504–2510, 2015, doi: 10.1039/c4ra12494d.

[2] T. P. Gujar, V. R. Shinde, C. D. Lokhande, R. S. Mane, and S. H. Han, “Formation of highly textured (1 1 1) Bi 2 O 3 films by anodization of electrodeposited bismuth films,” *Appl Surf Sci*, vol. 252, no. 8, pp. 2747–2751, 2006, doi: 10.1016/j.apsusc.2005.04.034.

[3] H. Kim, C. Jin, S. Park, W. I. Lee, I. J. Chin, and C. Lee, “Structure and optical properties of Bi2S3 and Bi2O3 nanostructures synthesized via thermal evaporation and thermal oxidation routes,” *Chemical Engineering Journal*, vol. 215–216, pp. 151–156, 2013, doi: 10.1016/j.cej.2012.10.102.

[4] Y.-J. Huang, Y.-Q. Zheng, H.-L. Zhu, and J.-J. Wang, “Hydrothermal synthesis of bismuth (III) coordination polymer and its transformation to nano α-Bi2O3 for photocatalytic degradation,” *J Solid State Chem*, vol. 239, pp. 274–281, 2016.

[5] A. Shokuhfar, A. Esmaeilirad, and V. Mazinani, “Synthesis and characterization of Bismuth oxide nanoparticles via sol-gel method,” no. January, 2014.

[6] S. E. Pratsinis, “Bismuth Oxide Nanoparticles by Flame Spray Pyrolysis,” vol. 18, pp. 1713–1718, 2002.

[7] L. Torrisi *et al.*, “Laser-generated bismuth nanoparticles for applications in imaging and radiotherapy,” *Journal of Physics and Chemistry of Solids*, vol. 119, pp. 62–70, 2018, doi: 10.1016/j.jpcs.2018.03.034.

[8] S. Anandan and J. J. Wu, “Microwave assisted rapid synthesis of Bi2O3 short nanorods,” *Mater Lett*, vol. 63, no. 27, pp. 2387–2389, 2009, doi: 10.1016/j.matlet.2009.08.022.

[9] Z. A. Zulkifli, K. A. Razak, W. N. W. A. Rahman, and S. Z. Abidin, “Synthesis and Characterisation of Bismuth Oxide Nanoparticles using Hydrothermal Method: The Effect of Reactant Concentrations and application in radiotherapy,” in *Journal of Physics: Conference Series*, IOP Publishing, 2018, p. 12103. doi: 10.1088/1742-6596/1082/1/012103.

[10] J. Wu, F. Qin, Z. Lu, H. J. Yang, and R. Chen, “Solvothermal synthesis of uniform bismuth nanospheres using poly(n-vinyl-2-pyrrolidone) as a reducing agent,” *Nanoscale Res Lett*, vol. 6, no. 1, pp. 1–8, 2011, doi: 10.1186/1556-276X-6-66.

[11] J. La, Y. Huang, G. Luo, J. Lai, C. Liu, and G. Chu, “Synthesis of bismuth oxide nanoparticles by solution combustion method,” *Particulate Science and Technology*, vol. 31, no. 3, pp. 287–290, 2013, doi: 10.1080/02726351.2012.727525.

[12] T. P. Gujar, V. R. Shinde, and C. D. Lokhande, “The influence of oxidation temperature on structural, optical and electrical properties of thermally oxidized bismuth oxide films,” *Appl Surf Sci*, vol. 254, no. 13, pp. 4186–4190, 2008, doi: 10.1016/j.apsusc.2008.01.040.

[13] R. Senthamilselvi and R. Velavan, “Microstructure and photocatalytic properties of bismuth oxide (Bi 2 O 3) nanocrystallites,” *Malaya Journal of Matematik*, vol. S, no. 2, pp. 4870–4874, 2020.

[14] A. Srivastava and A. Katiyar, “Zinc oxide nanostructures,” *Ceramic Science and Engineering: Basics to Recent Advancements*, pp. 235–262, Jan. 2022, doi: 10.1016/B978-0-323-89956-7.00012-7.

[15] I. L. Ikhioya *et al.*, “the Green Synthesis of Copper Oxide Nanoparticles Using the Moringa Oleifera Plant and Its Subsequent Characterization for Use in Energy Storage Applications,” *East European Journal of Physics*, vol. 2023, no. 1, pp. 162–172, 2023, doi: 10.26565/2312-4334-2023-1-20.

[16] E. N. Josephine, O. S. Ikponmwosa, and I. L. Ikhioya, “SYNTHESIS OF SnS/SnO NANOSTRUCTURE MATERIAL FOR PHOTOVOLTAIC APPLICATION,” *East European Journal of Physics*, vol. 2023, no. 1, pp. 154–161, 2023, doi: 10.26565/2312-4334-2023-1-19.

[17] I. L. Ikhioya, E. U. Onoh, D. N. Okoli, and A. J. Ekpunobi, “Impact of bismuth as dopant on ZnSe material syntheses for photovoltaic application,”

Materials Research Innovations, vol. 00, no. 00, pp. 1–9, 2023, doi: 10.1080/14328917.2023.2180582.

[18] I. L. Ikhioya, F. U. Ochai-Ejeh, and C. I. Uruwah, "Impact of modulated temperature on photovoltaic properties of automated spray fabricated zirconium doped cobalt selenide films," *Materials Research Innovations*, vol. 00, no. 00, pp. 1–10, 2023, doi: 10.1080/14328917.2023.2178747.

[19] K. I. Udofia, I. L. Ikhioya, A. U. Agobi, D. N. Okoli, and A. J. Ekpunobi, "Effects of zirconium on electrochemically synthesized tin selenide materials on fluorine doped tin oxide substrate for photovoltaic application," *Journal of the Indian Chemical Society*, vol. 99, no. 10, p. 100737, 2022, doi: 10.1016/j.jics.2022.100737.

[20] I. L. Ikhioya, G. M. Whyte, and A. C. Nkele, "Temperature-modulated nanostructures of ytterbium-doped Cobalt Selenide (Yb-CoSe) for photovoltaic applications," *Journal of the Indian Chemical Society*, vol. 100, no. 1, p. 100848, 2023, doi: 10.1016/j.jics.2022.100848.

[21] I. I. Lucky, U. F. C, and I. B. Okeghene, "Growth And Characterization Of Manganese Sulphide (MnS) Thin Films," *International Journal For Research In Applied And Natural Science*, vol. 4, no. 1, pp. 1–9, 2018.

[22] I. L. Ikhioya and A. J. Ekpunobi, "of NAMP Electrical and Structural Properties of ZnSe Thin Films by Electrodeposition Technique Journal of the Nigerian Association of Mathematical Physics © J . of NAMP Electrical and Structural Properties of ZnSe Thin Films by Electrodeposition Technique," no. March, 2015.

[23] I. L. Ikhioya and A. J. Ekpunobi, "Effect of Deposition Period and pH on Electrodeposition Technique of Zinc Selenide Thin Films Materials and Methods Results and Discussion Optical Properties of ZnSe Films," *Journal of the Nigerian Association of Mathematical Physics*, vol. 28, no. 2, pp. 281–288, 2014.

[24] I. I. Lucky, E. M. Chigozirim, O. Doris O, A. C. Rita, and O. C. Ogonnaya, "The Influence of Precursor Temperature on The Properties of Erbium-Doped Zirconium Telluride Thin Film Material Via Electrochemical Deposition," *International Journal of Applied Physics*, vol. 7, no. 1, pp. 102–109, 2020, doi: 10.14445/23500301/ijap-v7i1p115.

[25] I. I. Lucky, O. D.N, and E. A.J, "Effect Of Temperature On SnZnSe Semiconductor Thin Films For Photovoltaic Application," *International Journal of Applied Physics*, vol. 6, no. 2, pp. 55–67, 2019, doi: 10.14445/23500301/ijap-v6i2p109.

[26] I. L. Ikhioya, I. B. Okeoghene, A. C. B, O. N. Josephine, and A. Yahaya, "Effect of Precursor pHon Cadmium Doped Manganese Sulphide (CdMnS) Thin Films For Photovoltaic Application," *International Journal of Material Science and Engineering*, vol. 6, no. 2, pp. 1–8, 2020, doi: 10.14445/23948884/ijmse-v6i2p101.

[27] N. I. Akpu, A. A.D, N. L.A, and I. L. Ikhioya, "Investigation On The Influence of Varying Substrate Temperature On The Physical Features of Yttrium Doped Cadmium Selenide Thin Films Materials," *International Journal of Applied Physics*, vol. 8, no. 2, pp. 37–46, 2021, doi: 10.14445/23500301/ijap-v8i2p106.

[28] W. Raza, D. Bahnemann, and M. Muneer, "A green approach for degradation of organic pollutants using rare earth metal doped bismuth oxide," *Catal Today*, vol. 300, no. April 2017, pp. 89–98, 2018, doi: 10.1016/j.cattod.2017.07.029.

[29] A. Mathematics, "济無No Title No Title No Title," no. May, pp. 1–23, 2016.

[30] H. Chen *et al.*, "Synthesis of Li-doped bismuth oxide nanoplates, Co nanoparticles modification, and good photocatalytic activity toward organic pollutants," *Toxicol Environ Chem*, vol. 102, no. 7–8, pp. 356–385, 2020, doi: 10.1080/02772248.2020.1798448.

[31] S. K. T. Aziz *et al.*, "A Janus cerium-doped bismuth oxide electrocatalyst for complete water splitting," *Cell Rep Phys Sci*, vol. 3, no. 11, p. 101106, 2022, doi: 10.1016/j.xcrp.2022.101106.

[32] A. Dere, M. Soylu, and F. Yakuphanoglu, "Solar light sensitive photodiode produced using a coumarin doped bismuth oxide composite," *Mater Sci Semicond Process*, vol. 90, no. June 2018, pp. 129–142, 2019, doi: 10.1016/j.mssp.2018.10.009.

[33] S. Ohara and Y. Kuroiwa, "Highly ytterbium-doped bismuth-oxide-based fiber," vol. 17, no. 16, pp. 14104–14108, 2009.

[34] G. Zhang *et al.*, "Doping of Vanadium into Bismuth Oxide Nanoparticles for Electrocatalytic CO2Reduction," *ACS Appl Nano Mater*, vol. 5, no. 10, pp. 15465–15472, 2022, doi: 10.1021/acsanm.2c03503.

[35] P. S. Cardenas-Terrazas *et al.*, "High ionic conductivity dysprosium and tantalum Co-doped bismuth oxide electrolyte for low-temperature SOFCs," *Ionics (Kiel)*, vol. 26, no. 9, pp. 4579–4586, 2020, doi: 10.1007/s11581-020-03572-y.

[36] M. Mohammadi *et al.*, "Toxicity, morphological and structural properties of chitosan-coated Bi2O3-Bi(OH)3 nanoparticles prepared via DC arc discharge in liquid: A potential nanoparticle-based CT contrast agent," *Micro Nano Lett*, vol. 14, no. 3, pp. 239–244, 2019, doi: 10.1049/mnl.2018.5145.

[37] N. Motakef-Kazemi and M. Yaqoubi, "Green synthesis and characterization of bismuth oxide nanoparticle using mentha pulegium extract," *Iranian Journal of Pharmaceutical Research*, vol. 19, no. 2, pp. 70–79, 2020, doi: 10.22037/ijpr.2019.15578.13190.